# Precision Engineering of the Co-immobilization of Enzymes for Cascade Biocatalysis

Luo, Zhiyuan; Qiao, Li; Chen, Haomin; Mao, Zhili; Wu, Shujiao; Ma, Bianqin; Xie, Tian; Wang, Anming; Pei, Xiaolin; Sheldon, Roger A.

**DOI**
10.1002/anie.202403539

**Publication date**
2024

**Document Version**
Final published version

**Published in**
Angewandte Chemie - International Edition

How to cite: Angew. Chem. Int. Ed. 2024, e202403539
doi.org/10.1002/anie.202403539

Multienzyme Cascades

# Precision Engineering of the Co-immobilization of Enzymes for Cascade Biocatalysis

*Zhiyuan Luo, Li Qiao, Haomin Chen, Zhili Mao, Shujiao Wu, Bianqin Ma, Tian Xie, Anming Wang, Xiaolin Pei,* and Roger A. Sheldon*

**Abstract:** The design and orderly layered co-immobilization of multiple enzymes on resin particles remain challenging. In this study, the SpyTag/SpyCatcher binding pair was fused to the N-terminus of an alcohol dehydrogenase (ADH) and an aldo-keto reductase (AKR), respectively. A non-canonical amino acid (ncAA), *p*-azido-L-phenylalanine (p-AzF), as the anchor for covalent bonding enzymes, was genetically inserted into preselected sites in the AKR and ADH. Employing the two bioorthogonal counterparts of SpyTag/SpyCatcher and azide–alkyne cycloaddition for the immobilization of AKR and ADH enabled sequential dual-enzyme coating on porous microspheres. The ordered dual-enzyme reactor was subsequently used to synthesize (*S*)-1-(2-chlorophenyl)ethanol asymmetrically from the corresponding prochiral ketone, enabling the in situ regeneration of NADPH. The reactor exhibited a high catalytic conversion of 74 % and good reproducibility, retaining 80 % of its initial activity after six cycles. The product had 99.9 % ee, which that was maintained in each cycle. Additionally, the double-layer immobilization method significantly increased the enzyme loading capacity, which was approximately 1.7 times greater than that of traditional single-layer immobilization. More importantly, it simultaneously enabled both the purification and immobilization of multiple enzymes on carriers, thus providing a convenient approach to facilitate cascade biocatalysis.

[*] Dr. Z. Luo, Dr. L. Qiao, H. Chen, Z. Mao, B. Ma, Prof. A. Wang, Prof. X. Pei
College of Material, Chemistry and Chemical Engineering
Hangzhou Normal University, China
Hangzhou, Zhejiang, 311121, China
E-mail: pxl@hznu.edu.cn

S. Wu, Prof. T. Xie
School of Pharmacy
Hangzhou Normal University, China
Hangzhou, Zhejiang, 311121, China

Prof. R. A. Sheldon
Molecular Sciences Institute, School of Chemistry
University of the Witwatersrand
PO Wits. 2050, Johannesburg, South Africa

Prof. R. A. Sheldon
Department of Biotechnology, Section BOC
Delft University of Technology
Van der Maasweg 9, 2629 HZ Delft, The Netherlands

## Introduction

Multienzyme cascade reactions facilitate the execution of multistep reactions in a "one-pot" fashion, offering several advantages over the traditional batch reaction mode.[1] They minimize the accumulation of unstable and/or toxic intermediates, increase overall synthetic efficiency, avoid the purification of intermediates, and enable the in situ regeneration of cofactors, such as nicotinamide adenine dinucleotide (NADH), nicotinamide adenine dinucleotide phosphate (NADPH), and adenosine triphosphate (ATP).[2] These cofactors are stoichiometrically consumed, which is prohibitively expensive (e.g. NADPH, $2600/mol) for most industrial biocatalytic processes unless they are recycled by a second enzyme.[3] The utilization of multienzyme catalysis is considered to be an attractive approach for producing pharmaceuticals, biofuels, and fine chemicals.[4] For example, McIntosh et al. developed a three-enzyme cascade to synthesize molnupiravir (MK-4482), an investigational antiviral agent for the treatment of COVID-19, from ribose and uracil.[5] The synthesis yielded approximately 7 times more product than traditional chemical processes. The same group also developed an enzymatic cascade to synthesize MK-1454, a powerful stimulator of interferon genes (STING) protein, by utilizing a non-natural cofactor (thiotriphosphate) recycling system.[6] Similarly, Huffman et al. developed a biocatalytic cascade comprising five engineered enzymes and four coenzymes to stereoselectively synthesize islatravir, an investigational HIV therapeutic drug.[7] The overall yield from a simple achiral building block was 51 %. As a result of the evolution of enzymes and cofactor engineering, these entire processes were accomplished with a high yield of the target product under mild conditions without the need to isolate intermediates. These successes suggest that multienzyme cascade reactions have great potential in pharmaceutical manufacturing due to the excellent selectivity of synthetic reactions and the reduction of potential hazards.[8]

Currently, multienzyme cascade reactions still face numerous challenges, particularly in coordinating and reusing the cascaded enzymes.[9] The ability of enzymes to function in non-native environments, such as varying pH, temperature, and organic solvents, directly determines the catalytic efficiency of the cascade reaction process. Co-immobilization of enzymes, involving both carrier and carrier-free methods, has proven to be an excellent solution for scaling up biocatalytic cascades.[10] Carrier-based immobilization of enzymes is a conventional yet appealing

strategy due to their excellent hydrodynamics, especially with innovative nanomaterials like metal–organic frameworks (MOFs), covalent-organic frameworks (COFs), and biopolymers.[11] For example, Paul et al. synthesized an ordered 2D COF-foam nanostructure to immobilize β-glucosidase and cellobiohydrolase for the tandem conversion of carboxymethylcellulose to glucose with high catalytic efficiency and recyclability (10 cycles).[12] Similarly, Ren et al. constructed a nanoscale multienzyme reactor by co-encapsulating carbonic anhydrase, formate dehydrogenase, glutamate dehydrogenase, and cofactor NADH in zeolitic imidazolate framework-8 (ZIF-8). The reactor exhibited an outstanding conversion efficiency from $CO_2$ to formate, with the yield increased by 4.6 times that of the free multienzyme system.[13] Zhang et al. engineered the microcompartment protein EutM to self-assemble as structural scaffolds using SpyTag-SpyCatcher covalent bond formation technology.[14] Alcohol dehydrogenase and amine dehydrogenase were co-immobilized on the film surface to form a dual-enzyme cascade for chiral amine synthesis from the corresponding alcohol, resulting in an excellent enantiomeric excess (> 99 %) and high catalytic efficiency. The most straightforward strategy for multienzyme co-immobilization is currently spontaneous assembly in a randomized manner. However, the cooperativity of multiple immobilized enzymes and the control of their immobilization mode still present significant challenges.[15] Positional co-immobilization and compartmentalization have been utilized to facilitate enzyme assembly following the reaction pathway, enabling the customization and optimization of channels and surfaces for enzymatic cascade reactions.[16] Nevertheless, there is currently no simple and general strategy for the co-immobilization of multiple enzymes that is rapid and allows for controllable positions and orientations, ordered ligation, strong covalent bonding, and high protein loading.

Recently, the carrier-free immobilization of multiple enzymes using bioorthogonal chemistry has attracted extensive interest due to its convenient operability.[17] In our previous work, we constructed a nano-reactor with a multi-enzyme assembly to synthesize chiral pharmaceutical intermediates by incorporating non-canonical amino acids (ncAAs) into enzymes.[18] In this work, we proposed a dual-enzyme ordered coating strategy that combines the advantages of carrier and carrier-free immobilization. A dual-enzyme cascade system was developed to synthesize (*S*)-1-(2-chlorophenyl)ethanol from *o*-chloroacetophenone by regenerating the cofactor NADPH in situ. This system involved an alcohol dehydrogenase (ADH) and aldo-keto reductase (AKR) as model enzymes, which were sequentially anchored on the surface of porous P(GMA-EDMA) organic polymer microspheres (Figure 1). The two enzymes were combined through the spontaneous cross-linking of the SpyTag/SpyCatcher system and then immobilized via a click reaction between the inserted ncAA-bearing azide groups and the vector functionalized with alkyne groups. The spatial arrangement of the two enzymes can be controlled on the solid supports. The strategy can also simultaneously achieve the purification and immobilization of target enzymes.

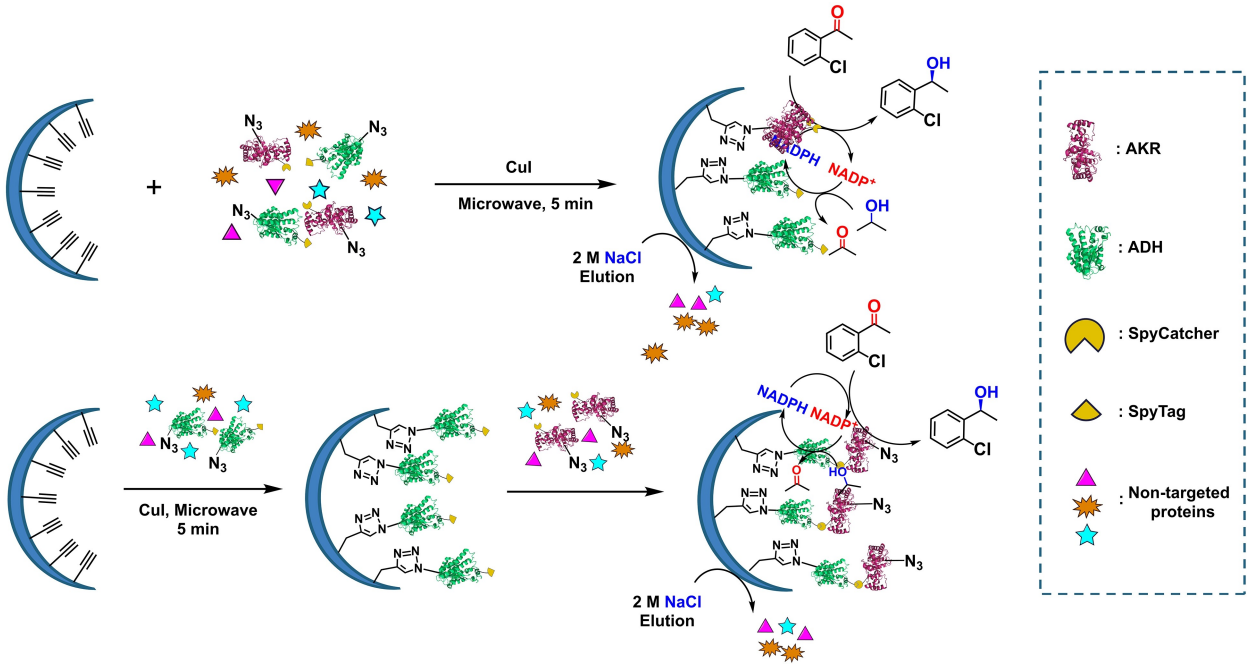


***Figure 1.*** Dual-enzyme coating of porous microspheres. a) Randomized dual-enzyme monolayered coating. b) Ordered double-layered dual-enzyme coating.

## Results and Discussion

### Construction of Fused Enzymes and Their Mutants

The reaction system of AKR and ADH can efficiently synthesize chiral alcohols from ketones coupled with NADPH regeneration.[19] The SpyTag/SpyCatcher (ST/SC) system is a site-specific protein coupling reaction that occurs through intermolecular isopeptide binding.[20] To covalently ligate AKR with ADH, the SpyTag and SpyCatcher peptides were fused to the C-terminus or N-terminus of AKR and ADH, respectively. Unfortunately, attempting to fuse a SpyTag to the C-terminus of ADH greatly diminished its catalytic activity. ADH is a NADP-dependent short-chain reductase with catalytic activity dependent on $Mg^{2+}$.[21] When the C-terminus of ADH is attached to the SpyTag peptide, it leads to the loss of $Mg^{2+}$ and/or hinders the catalytic reaction. Thus, we fused the SpyTag and the SpyCatcher to the N-terminus of ADH and AKR, respectively, using a flexible peptide of GSGGSG as a linker. The theoretical molecular weights of fused AKR and ADH were 45.0 kDa and 29.7 kDa, respectively. The results of sodium dodecyl sulfate-polyacrylamide gel electrophoresis (SDS-PAGE) and matrix-assisted laser desorption/ionization time-of-flight mass spectrometry (MALDI-TOF-MS) confirmed the successful expression of recombinant ST-ADH and SC-AKR (Figures S4 and S5).

To immobilize ST-ADH or SC-AKR on porous microspheres in a specific orientation, we inserted a *p*-azido-L-phenylalanine as the ncAA into both proteins by genetic code expansion. The codons of the preselected sites on the surface of AKR and ADH were mutated to UAG. The (GRO)-ΔA strain of *Escherichia coli* MG1655 can incorporate synonymous UAA codons instead of all known UAG stop codons.[22] This enables the deletion of release factor 1 (RF1) and the redistribution of translation function of UAG. The genome-recoded strain eliminates the UAG termination function in *E.* coli and only produces the UAA termination codon linkage. In addition, plasmid pEVOL was used in MG1655 to host the evolved aminoacyl-tRNA synthetase (aaRS)/suppressor tRNA pairs derived from *Methanocaldococcus jannaschii* to identify non-canonical amino acids (ncAAs). The aaRS/tRNA pairs in the pEVOL vector ensure that ncAAs are incorporated with high fidelity only in response to the nonsense codon UAG, and do not encode endogenous amino acids in response to other codons. The selected mutant sites for AKR and ADH are shown in Figure S1. Based on our previous studies, the mutant sites for AKR were identified as 130S, 162Q, 189Q, and 232W, and these sites were 104A, 125I, 155Y, 199P, and 204A for ADH.[18,23] The selection principles for mutation sites are as follows. 1) far from the active center; 2) less impact on the protein structure, considering similar group size or electronegativity; 3) located on the surface of a protein.

These variants with different fused tags were expressed in *E. coli* MG1655 (Table S6 and S7). The SC-AKR 232W variant exhibited higher expression levels and better specific activity compared to the wild-type fused enzyme SC-AKR (Figure 2a). The ST-ADH 104A variant exhibited the highest specific activity, and its expression level was comparable to that of the wild-type ST-ADH (Figure 2b). Therefore, SC-AKR 232W and ST-ADH 104A were selected as the optimum variants for future work. The results of MALDI-TOF-MS analyses are consistent with the theoretical molecular weight of SC-AKR 232W and ST-ADH 104A (Figure 2d,e).

To confirm the cross-linking between AKR and ADH variants using SpyTag/SpyCatcher, SC-AKR 232W (lane 1) and ST-ADH 104A (lane 2) were mixed at a molar ratio of 3:1 and incubated for 2 h (lane 3) and 4 h (lane 4) at 18 °C (Figure 2c). The red box indicates the dual-enzyme complex formed by cross-linking, implying that most of ST-ADH 104A was cross-linked with SC-AKR 232W after reacting for 4 hours. Thus, the cross-linking reaction between SpyTag and SpyCatcher is efficient for the covalent linkage of AKR and ADH under mild conditions.

### Preparation and Activation of Porous Resins

To acquire appropriate solid carriers, porous polymer resins with a macroporous structure were synthesized using the reverse micelle swelling technique. Glycidyl methacrylate (GMA) and ethylene glycol dimethacrylate (EDMA) were employed as monomers in the polymerization process, and sorbitan oleate (Span 80) was used as a porogenic agent. The average particle size of the obtained resins was influenced by the stirring speed during the preparation, while the pore size was related to the added amount of Span 80. The surface of microspheres was smooth and non-porous in the absence of Span 80 surfactant (Figure S9).

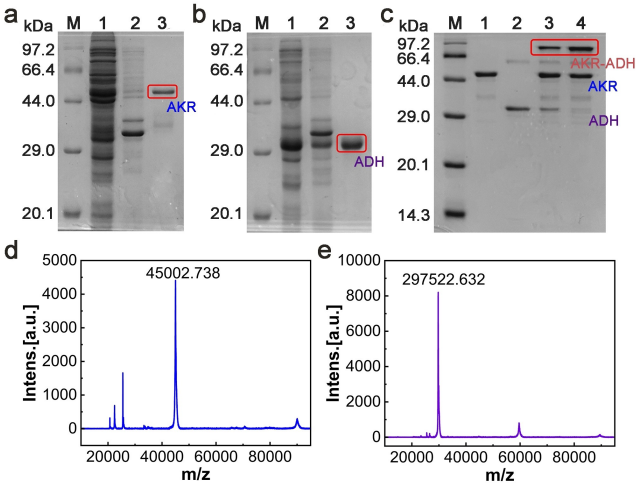


***Figure 2.*** Expression and cross-linking of AKR and ADH variants. a) SDS-PAGE of SC-AKR 232W. b) SDS-PAGE of ST-ADH 104A (M, marker; lanes 1, 2, and 3 are supernatant, precipitate, and pure enzyme solution of cell lysate respectively). c) SDS-PAGE of mixed enzyme solution of purified SC-AKR 232W and ST-ADH 104A (M, marker; lane 1 is SC-AKR 232W; lane 2 is ST-ADH 104A; lanes 3 and 4 are mixed solutions at 2 h and 4 h, respectively). d) MALDI-TOF MS analysis of SC-AKR 232W. e) MALDI-TOF MS analysis of ST-ADH 104A.

When Span 80 was added to 25 % of the total monomer mass (GMA and EDMA combined), the obtained resin exhibited an excellent surface pore structure with regular shapes. By increasing the amount of Span 80 to 27.5 %, the microspheres began to break down, resulting in an irregular surface with poor shape. This occurred because an excessive amount of surfactant caused the oil droplets to absorb a large amount of water, leading to the failure of the polymer resin to solidify.[24]

The chemical groups on the porous resins were subsequently functionalized as shown in Figure 3a. The epoxy groups were first aminated with 1,3-diaminopropane, followed by reaction with 2-((prop-2-yn-1-yloxy)methyl)oxirane to produce an alkynyl group as the anchor to covalently immobilize enzymes. The surface and pore structure of the microspheres were observed through scanning electron microscopy (SEM) analysis (Figure 3b,c). Clearly, a great number of pores were distributed on the surface of microspheres. The most accessible pore size of the resin was measured to be 50.4 nm using mercury intrusion porosimetry (MIP; Figure 3d). Furthermore, the characteristic absorption peaks at 3287 $cm^{-1}$ and 2119 $cm^{-1}$ indicate the stretching vibrations of ≡C–H and –C≡C groups, respectively (red curve in Figure 3e).[25] The results indicate that the resins were successfully activated via amination and alkynylation.

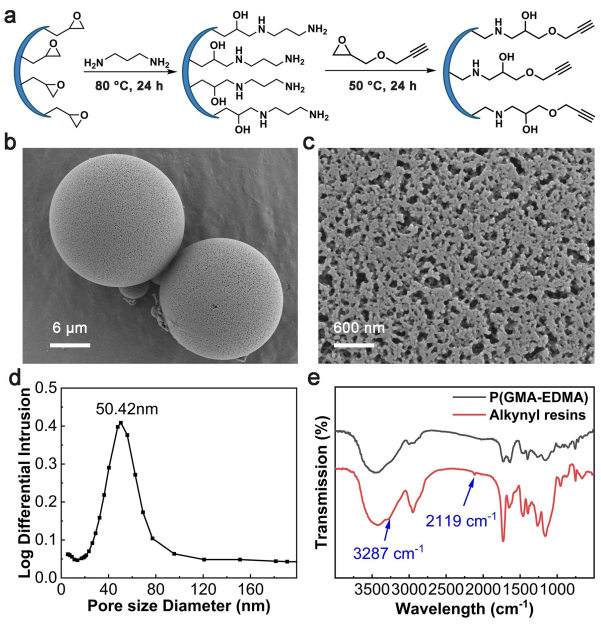


***Figure 3.*** Preparation and structure analysis of porous microspheres. a) SEM image of porous microspheres. b) SEM image of the surface pores of the microspheres. c) The most accessible pore size of the microspheres measured by MIP. d) FTIR analysis of the alkyne-based resin.

### *Precise Dual-Enzyme Coating on Porous Resins*

The variants of AKR and ADH were individually immobilized through a click reaction between the *p*-azido-L-phenylalanine and the alkynyl groups on the porous microspheres. The linkage occurred when SC-AKR 232W and the alkyne-functionalized resins underwent microwave-assisted click chemistry in the presence of a CuI catalyst. Subsequently, the resins containing SC-AKR 232W were cross-linked with ST-ADH 104A after incubating and shaking at 18 °C for 3 h. Thus, AKR and ADH were sequentially coated on resin particles to form an orderly dual-enzyme "coating". We varied the spatial location of the two enzymes by changing the order of SC-AKR 232W and ST-ADH 104A in the coating process. Meanwhile, to prepare the disordered single-layer immobilization as the control, ST-ADH 104A and SC-AKR 232W were directly mixed with resins, and immobilized with microwave assistance. In this case, AKR and ADH were directly fixed on resins using click chemistry.

To confirm the successful immobilization of enzymes on the resin, the microstructure was investigated using SEM and energy-dispersive spectrometry (EDS). The results show that the pore channels on the resin surface remain intact after the proteins are immobilized, indicating that the immobilized enzyme did not block the pore channels (Figure S11). Furthermore, the observation of the widespread distribution of sulphur (S) atoms on the resin surface indicated the successful immobilization of enzymes with the S atoms of cysteine residues (Figure S12).

To determine the protein loading on resins, the immobilization was carried out using pure enzyme solutions of ST-ADH 104A and SC-AKR 232W. The dual-enzyme coating of @$\frac{\text{ADH}}{\text{AKR}}$ contained 174.88 mg of protein per gram of resin, which is 1.69 times higher than the protein loading achieved in the disordered monolayer immobilization of @$\frac{\text{AKR}}{\text{ADH}}$ (103.67 mg/g). The results suggest that the enzyme loading on the resin can be significantly increased through bilayer immobilization.

To further demonstrate the ordered arrangement of AKR and ADH on resins, we used two distinct fluorescent probes to label the two enzymes separately (Figure 4a). The histidine tag (His-tag) of ST-ADH was replaced by a cysteine tag with a short peptide sequence of C–C–X–X–C–C using the polymerase chain reaction (PCR), where X can represent any amino acid except cysteine. The cysteine residues on this tag were specifically recognized and bound by two As(III) ions on the double arsenic fluorescein FlAsH-$EDT_2$, causing the enzyme to fluoresce green in the wavelength range of 577–492 nm.[26] The His-tag of SC-AKR was labelled with a Cy5-BisNTA–Ni fluorescent probe, which emitted red fluorescence when irradiated with wavelengths ranging from 770 nm to 622 nm.[27]

To visualize dual-enzyme "coatings" of @ADH-AKR and @AKR-ADH, SC-AKR 232W (with a His tag) and ST-ADH 104A (with a Cys tag) were immobilized on the resins in different sequences. After specific labeling of AKR and ADH using FlAsH-$EDT_2$ and Cy5-BisNTA–Ni, respec-

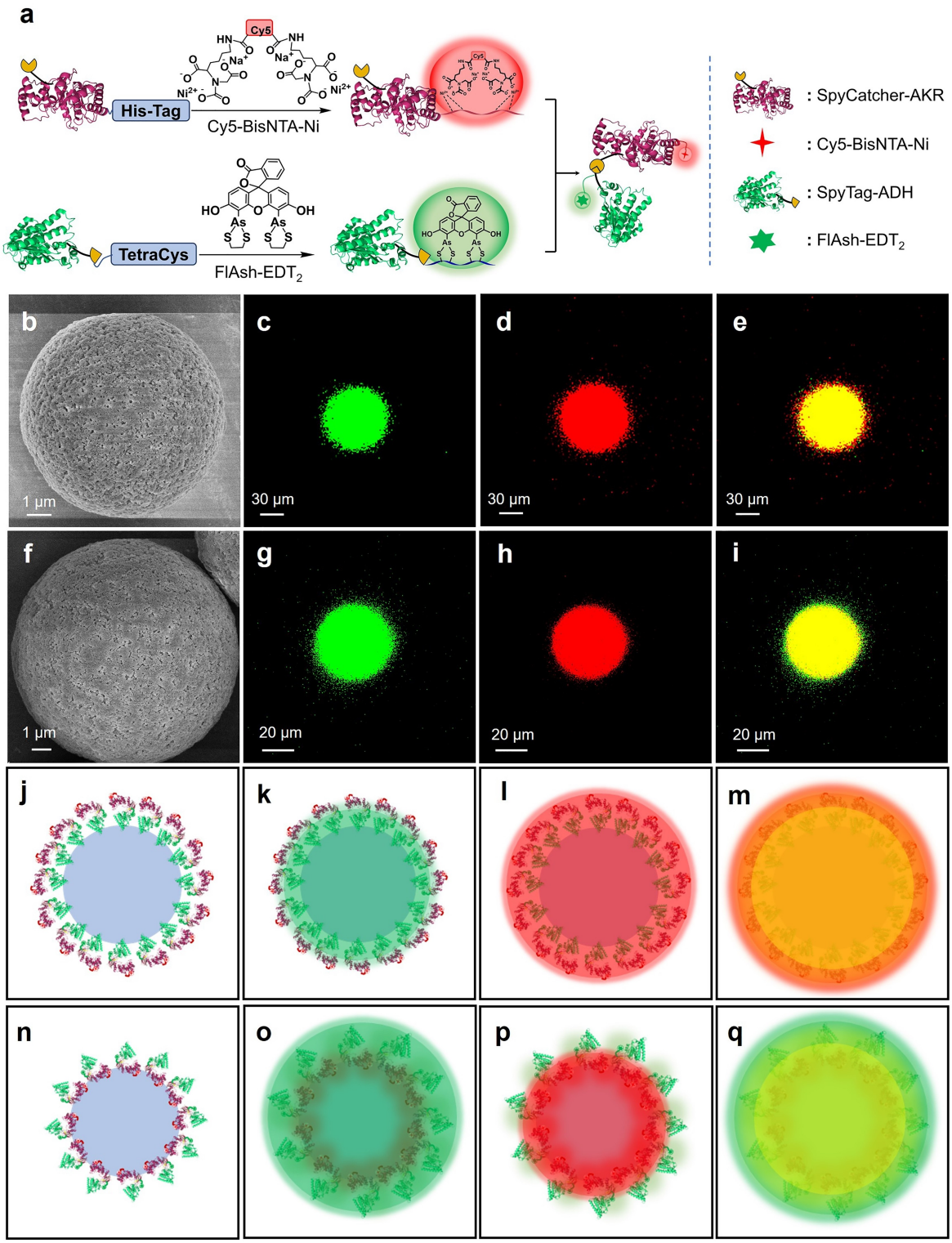


***Figure 4.*** Construction and characterization of a dual-enzyme coating. a) Specific fluorescence labelling of AKR and ADH, respectively. b) SEM image of @ADH-AKR. c) CLSM image of @ADH-AKR in the wavelength range of 577–492 nm. d) CLSM image of @ADH-AKR in the wavelength range of 770–622 nm. e) CLSM image of @ADH-AKR in the wavelength range of 577–492 nm and 770–622 nm. f) SEM image of @AKR-ADH. g) CLSM image of @AKR-ADH in the wavelength range of 577–492 nm. h) CLSM image of @AKR-ADH in the wavelength range of 770–622 nm. i) CLSM image of @AKR-ADH in the wavelength range of 577–492 nm and 770–622 nm. j-m) Schematic of fluorescence luminescence of @ADH-AKR without fluorescence, 577–492 nm, 770–622 nm, and dual-wavelength channels, respectively. n-q) Schematic of fluorescence luminescence of @AKR-ADH without fluorescence, 577–492 nm, 770–622 nm and dual-wavelength channels, respectively.

tively, the coated dual-enzyme reactors were observed using scanning electron microscopy (SEM; Figure 4b,f) and confocal laser scanning microscopy (CLSM). For @ADH-AKR, the ST-ADH 104A in the inner layer appears green at 577–492 nm (Figure 4c), and the SC-AKR 232W in the outer layer appears red at 770–622 nm (Figure 4d). The resins appeared in a mixed red-green color (yellow) when both excitation channels were open (Figure 4e), indicating that both AKR and ADH were successfully coated and evenly distributed on the carriers. In particular, there is a red fluorescence ring outside the yellow circle. The observation represents the SC-AKR 232W fixed in the outer layer of the resin, which is consistent with the spatially ordered structure of the dual-enzyme coating (Figure 4j–m). Similarly, in the dual-enzyme coating of @AKR-ADH, the outer layer with the ST-ADH 104A exhibits a green emission (Figure 4g), while the inner layer of the SC-AKR 232W exhibits a red emission (Figure 4h). The green fluorescence ring on the outer layer of the mixed yellow light in the dual-channel combination diagram is caused by the ST-ADH coating on the outer layer (Figure 4i). Hence, the outer ring of the dual enzyme coating exhibits red fluorescence when AKR is encapsulated in the inner layer, and green fluorescence when ADH is encapsulated in the outer layer (Figure 4n–q). These results demonstrated the dual enzyme coating on the resin with an orderly bilayered structure.

### *Asymmetric Synthesis of (S)-1-(2-Chlorophenyl)ethanol*

(*S*)-1-(2-Chlorophenyl)ethanol is a crucial chiral building block for pharmaceuticals and is synthesized through the asymmetric reduction of *o*-chloroacetophenone by AKR. We investigated the apparent kinetics of ordered dual-enzyme coating of @ADH-AKR, @AKR-ADH, and disorderly co-immobilized @$\frac{\text{AKR}}{\text{ADH}}$ by measuring the change in NADPH absorbance at 340 nm using *o*-chloroacetophenone as the substrate. The dual-enzyme coating @AKR-ADH exhibits lower $K_m$ values and better catalytic efficiency, with a $K_{cat}/K_m$ value 2.1 times higher than that of @$\frac{\text{AKR}}{\text{ADH}}$ (Table 1). The catalytic performance of the immobilized enzymes can be influenced by the microenvironment around them, which is affected by macromolecular crowding and surface charge.[28]

Thermogravimetric analysis (TGA) was conducted on the immobilized enzymes (Figure 5a). The loss of mass over the temperature range of 0–115 °C can be attributed to the adsorbed water in the samples. Compared with the pure resin, the onset of weight loss temperatures for @ADH-AKR and @AKR-ADH was slightly lower, but the trend of the TGA curves essentially overlapped. The extra loss of @ADH-AKR and @AKR-ADH over the temperature range of 200–390 °C could be the pyrolysis of immobilized enzymes. In contrast, the onset temperature for weight loss of @$\frac{\text{ADH}}{\text{AKR}}$ was lower and lagged far behind that of the pure resin. Thus, the disordered fixing was more damaging to the thermal stability of the resin than the ordered coating.

To investigate the cyclic property of the coated dual enzymes, we individually performed the ordered coating of @ADH-AKR, @AKR-ADH, and the disorderly co-immobilized @$\frac{\text{AKR}}{\text{ADH}}$ to catalyze the reduction of *o*-chloroacetophenone at 30 °C for 10 h. In the asymmetric synthesis of (*S*)-1-(2-chlorophenyl) ethanol from *o*-chloroacetophenone, AKR is involved in the reduction of the ketone, while ADH is involved in the regeneration of NADPH (Figure S3). The immobilized enzymes were collected by centrifugation for

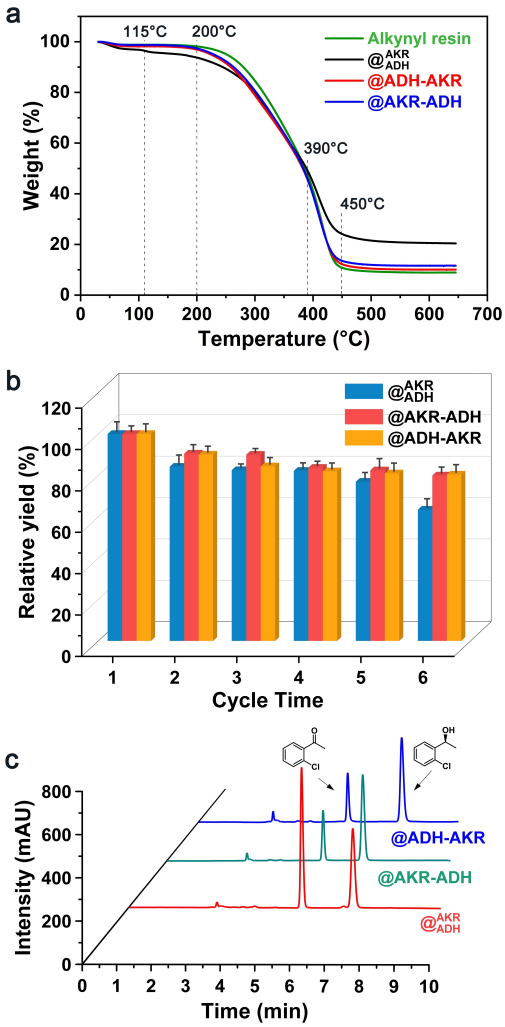


***Figure 5.*** Characterization of the immobilized enzymes. a) thermogravimetric analysis (TGA) characterization of the ordered coatings. b) Cyclic stability of @ADH-AKR, @AKR-ADH and @$\frac{\text{AKR}}{\text{ADH}}$. c) HPLC analysis of the product catalyzed by @ADH-AKR, @AKR-ADH, and @$\frac{\text{AKR}}{\text{ADH}}$).

***Table 1:*** Apparent kinetic analysis of ordered dual enzyme coated @ADH-AKR@AKR-ADH and disorderly co-immobilized **@AKR ADH**.

| Immobilization manner | $K_m$ (mM)[a] | $K_{cat}$ ($s^{-1}$) | $K_{cat}/K_m$ |
|---|---|---|---|
| @ADH-AKR | 0.178 ± 0.091 | 0.368 ± 0.020 | 2.067 |
| @AKR-ADH | 0.159 ± 0.076 | 0.435 ± 0.041 | 2.736 |
| @$\frac{\text{AKR}}{\text{ADH}}$ | 0.217 ± 0.076 | 0.277 ± 0.048 | 1.276 |

[a] Concentration of *o*-chloroacetophenone was in the range of 0.1–15 mM.

use in the following catalytic reaction. After 6 cycles of the catalytic reaction for a continuous 60 h, the conversion of @ADH-AKR and @AKR-ADH remained at approximately 80 % of their initial activities. However, the conversion of the disorderly co-immobilized dual-enzyme @$\frac{AKR}{ADH}$ retained the initial 63.4 % (Figure 5b). The disorderly co-immobilized dual-enzyme @$\frac{AKR}{ADH}$ resulted in a 41.6 % conversion rate and an enantiomeric excess (*e.e.*) of 98.6 % (Figure 5c). As expected, the (*S*)-1-(2-chlorophenyl) ethanol yield with @ADH-AKR as catalyst increased to 73.7 %, which is 1.77 times higher than that catalyzed by @$\frac{AKR}{ADH}$, and the same as that catalyzed by @AKR-ADH (73.7 %). It's worth noting that the *e.e.* values of the synthesized chiral alcohol catalyzed by the ordered dual-enzyme coatings were above 99.9 % (Figure 5c). Thus the ordered dual-enzyme reactor can efficiently perform the cascade reaction to synthesize the chiral alcohol. The regeneration of NADPH is a critical factor in the cascade reaction for synthesizing (*S*)-1-(2-chlorophenyl) ethanol, and its recycling shuttles between AKR and ADH. The excellent catalytic efficiency of the ordered coating enzymes is attributed to the proximity of $NADP^+$/NADPH channeling to the enzyme molecule.[29]

## Conclusion

In summary, we have developed a convenient method for the precise and orderly coating of multiple enzymes onto resin particles. The method is broadly applicable for the bioorthogonal covalent immobilization of multiple enzymes to enhance protein loading, rigidity, and stability, ensuring the vectorial catalysis of multienzyme cascades. The specific attachment of AKR to ADH ensures that their active sites are in close proximity, facilitating the control of their spatial position on the walls of resin pores. This results in an increase in the catalytic efficiency of the dual-enzyme reactor. Bioorthogonal chemistry enables one-step purification and immobilization from cell lysate supernatants. As compared to traditional monolayer co-immobilization, this multienzyme coating strategy offers the advantage of increasing the load capacity of the carrier and has potentially broad applications in biocatalytic cascades.

## Acknowledgements

This study was supported by the National Natural Science Foundation of China (22078079, 22378091, 22378092), the Natural Science Foundation of Zhejiang Province (LY18B060009, LY22B060003), and the Program for Postgraduates in Innovation Practice and Service for Locality" in HZNU (2022).

## Conflict of Interest

The authors declare no conflict of interest.

## Data Availability Statement

The data that support the findings of this study are available in the supplementary material of this article.

**Keywords:** enzymatic cascades · biological orthogonality · ordered immobilization · asymmetric reduction

[1] a) R. A. Sheldon, J. M. Woodley, *Chem. Rev.* **2018**, *118*, 801–838; b) Y. Zhou, S. Wu, J. Mao, Z. Li, *ChemSusChem* **2018**, *11*, 2221–2228; c) C. T. Walsh, B. S. Moore, *Angew. Chem. Int. Ed.* **2019**, *58*, 6846–6879; d) K. Tian, Z. Li, *Angew. Chem. Int. Ed.* **2020**, *59*, 21745–21751; e) S. K. Wu, R. Snajdrova, J. C. Moore, K. Baldenius, U. T. Bornscheuer, *Angew. Chem. Int. Ed.* **2021**, *60*, 88–119; f) A. R. Alcántara, P. D. de María, J. A. Littlechild, M. Schürmann, R. A. Sheldon, R. Wohlgemuth, *ChemSusChem* **2022**, *15*, e202102709; g) P. Q. Luan, Y. X. Li, C. Huang, L. L. Dong, T. Ma, J. Q. Liu, J. Gao, Y. T. Liu, Y. J. Jiang, *ACS Catal.* **2022**, *12*, 7550–7558.

[2] a) S. Schlager, L. M. Dumitru, M. Haberbauer, A. Fuchsbauer, H. Neugebauer, D. Hiemetsberger, A. Wagner, E. Portenkirchner, N. S. Sariciftci, *ChemSusChem* **2016**, *9*, 631–635; b) P. Gruber, M. P. C. Marques, B. O'Sullivan, F. Baganz, R. Wohlgemuth, N. Szita, *Biotechnol. J.* **2017**, *12*, 1700030.

[3] a) C. J. Hartley, C. C. Williams, J. A. Scoble, Q. I. Churches, A. North, N. G. French, T. Nebl, G. Coia, A. C. Warden, G. Simpson, A. R. Frazer, C. N. Jensen, N. J. Turner, C. Scott, *Nat. Catal.* **2019**, *2*, 1006–1015; b) J. W. H. Burnett, Z. Sun, J. Li, X. Wang, X. Wang, *Green Chem.* **2021**, *23*, 7162–7169; c) F. Gao, G. Liu, A. Chen, Y. Hu, H. Wang, J. Pan, J. Feng, H. Zhang, Y. Wang, Y. Min, C. Gao, Y. Xiong, *Nat. Commun.* **2023**, *14*, 6783; d) J. W. H. Burnett, R. F. Howe, X. Wang, *Trends Chem.* **2020**, *2*, 488–492.

[4] a) D. K. Gao, W. Song, J. Wu, L. Guo, C. Gao, J. Liu, X. L. Chen, L. M. Liu, *Angew. Chem. Int. Ed.* **2022**, e202207077; b) E. L. Bell, W. Finnigan, S. P. France, A. P. Green, M. A. Hayes, L. J. Hepworth, S. L. Lovelock, H. Niikura, S. Osuna, E. Romero, K. S. Ryan, N. J. Turner, S. L. Flitsch, *Nat. Rev. Method. Prime.* **2021**, *1*, 46; c) H. Dong, W. Zhang, S. Zhou, H. Ying, P. Wang, *ChemSusChem* **2022**, *15*, e202200850.

[5] J. A. McIntosh, T. Benkovics, S. M. Silverman, M. A. Huffman, J. Kong, P. E. Maligres, T. Itoh, H. Yang, D. Verma, W. L. Pan, H. I. Ho, J. Vroom, A. M. Knight, J. A. Hurtak, A. Klapars, A. Fryszkowska, W. J. Morris, N. A. Strotman, G. S. Murphy, K. M. Maloney, P. S. Fier, *ACS Cent. Sci.* **2021**, *7*, 1980–1985.

[6] J. A. McIntosh, Z. J. Liu, B. M. Andresen, N. S. Marzijarani, J. C. Moore, N. M. Marshall, M. Borra-Garske, J. V. Obligacion, P. S. Fier, F. Peng, J. H. Forstater, M. S. Winston, C. H. An, W. Chang, J. Lim, M. A. Huffman, S. P. Miller, F. R. Tsay, M. D. Altman, C. A. Lesburg, D. Steinhuebel, B. W. Trotter, J. N. Cumming, A. Northrup, X. D. Bu, B. F. Mann, M. Biba, K. Hiraga, G. S. Murphy, J. N. Kolev, A. Makarewicz, W. L. Pan, I. Farasat, R. S. Bade, K. Stone, D. Duan, O. Alvizo, D. Adpressa, E. Guetschow, E. Hoyt, E. L. Regalado, S. Castro, N. Rivera, J. P. Smith, F. Q. Wang, A. Crespo, D. Verma, S. Axnanda, Z. E. X. Dance, P. N. Devine, D. Tschaen, K. A. Canada, P. G. Bulger, B. D. Sherry, M. D. Truppo, R. T. Ruck, L. C. Campeau, D. J. Bennett, G. R. Humphrey, K. R. Campos, M. L. Maddess, *Nature* **2022**, *603*, 439–444.

[7] M. A. Huffman, A. Fryszkowska, O. Alvizo, M. Borra-Garske, K. R. Campos, K. A. Canada, P. N. Devine, D. Duan, J. H. Forstater, S. T. Grosser, H. M. Halsey, G. J. Hughes, J. Jo, L. A. Joyce, J. N. Kolev, J. Liang, K. M. Maloney, B. F. Mann, N. M. Marshall, M. McLaughlin, J. C. Moore, G. S. Murphy,

C. C. Nawrat, J. Nazor, S. Novick, N. R. Patel, A. Rodriguez-Granillo, S. A. Robaire, E. C. Sherer, M. D. Truppo, A. M. Whittaker, D. Verma, L. Xiao, Y. Xu, H. Yang, *Science* **2019**, *366*, 1255–1259.

[8] a) M. Pfeiffer, A. Ribar, B. Nidetzky, *Nat. Commun.* **2023**, *14*, 2261; b) R. A. Sheldon, *Green Chem.* **2023**, *25*, 1704–1728; c) A. I. Benitez-Mateos, D. R. Padrosa, F. Paradisi, *Nat. Chem.* **2022**, *14*, 489–499; d) M. Lubberink, C. Schnepel, J. Citoler, S. R. Derrington, W. Finnigan, M. A. Hayes, N. J. Turner, S. L. Flitsch, *ACS Catal.* **2020**, *10*, 10005–10009; e) U. Hanefeld, F. Hollmann, C. E. Paul, *Chem. Soc. Rev.* **2022**, *51*, 594–627.

[9] a) Y. Y. Qiao, W. Y. Ma, S. J. Zhang, F. Guo, K. Liu, Y. J. Jiang, Y. X. Wang, F. X. Xin, W. M. Zhang, M. Jiang, *Synth. Syst. Biotechnol.* **2023**, *8*, 578–583; b) L. Kuschmierz, L. Shen, C. Bräsen, J. Snoep, B. Siebers, *Curr. Opin. Biotechnol.* **2022**, *74*, 55–60.

[10] a) J. M. Bolivar, J. M. Woodley, R. Fernandez-Lafuente, *Chem. Soc. Rev.* **2022**, *51*, 6251–6290; b) M. Liu, Y. Song, Y. H. P. J. Zhang, C. You, *ChemSusChem* **2023**, *16*, e202202153; c) Z. Tan, H. Cheng, G. Chen, F. Ju, J. Fernández-Lucas, J. Zdarta, T. Jesionowski, M. Bilal, *Int. J. Biol. Macromol.* **2023**, *227*, 535–550; d) S. P. France, L. J. Hepworth, N. J. Turner, S. L. Flitsch, *ACS Catal.* **2017**, *7*, 710–724; e) K. Xu, X. Chen, R. Zheng, Y. Zheng, *Front. Bioeng. Biotech.* **2020**, *8*, 660.

[11] a) D. P. Tian, R. P. Hao, X. M. Zhang, H. Shi, Y. W. Wang, L. F. Liang, H. C. Liu, H. Q. Yang, *Nat. Commun.* **2023**, *14*, 3226; b) X. Pei, Y. Wu, J. Wang, Z. Chen, W. Liu, W. Su, F. Liu, *Nanoscale* **2020**, *12*, 967–972; c) Q. Zhu, Y. Zheng, Z. Zhang, Y. Chen, *Nat. Protoc.* **2023**, *18*, 3080–3125; d) M. C. Feng, Z. R. Niu, C. Y. Xing, Y. H. Jin, X. Feng, Y. Y. Zhang, B. Wang, *Angew. Chem. Int. Ed.* **2023**, *62*, e202306621; e) S. Ren, C. Li, X. Jiao, S. Jia, Y. Jiang, M. Bilal, J. Cui, *Chem. Eng. J.* **2019**, *373*, 1254–1278.

[12] S. Paul, M. Gupta, K. Dey, A. K. Mahato, S. Bag, A. Torris, E. B. Gowd, H. Sajid, M. A. Addicoat, S. Datta, R. Banerjee, *Chem. Sci.* **2023**, *14*, 6643–6653.

[13] S. Z. Ren, Z. Y. Wang, M. Bilal, Y. X. Feng, Y. H. Jiang, S. R. Jia, J. D. Cui, *Int. J. Biol. Macromol.* **2020**, *155*, 110–118.

[14] G. Q. Zhang, M. B. Quin, C. Schmidt-Dannert, *ACS Catal.* **2018**, *8*, 5611–5620.

[15] a) E. T. Hwang, S. Lee, *ACS Catal.* **2019**, *9*, 4402–4425; b) A. A. Júnior, Y. F. Ladeira, A. D. França, R. O. Souza, A. H. Moraes, R. Wojcieszak, I. Itabaiana, A. S. Miranda, *Catalysts* **2021**, *11*, 936.

[16] a) Y. Chen, G. Ke, Y. Ma, Z. Zhu, M. Liu, Y. Liu, H. Yan, C. J. Yang, *J. Am. Chem. Soc.* **2018**, *140*, 8990–8996; b) J. Liang, K. Liang, *Chem. Rec.* **2020**, *20*, 1100–1116.

[17] a) X. L. Pei, Z. Y. Luo, L. Qiao, Q. J. Xiao, P. F. Zhang, A. M. Wang, R. A. Sheldon, *Chem. Soc. Rev.* **2022**, *51*, 7281–7304; b) H. M. Li, R. Wang, A. M. Wang, J. Zhang, Y. C. Yin, X. L. Pei, P. F. Zhang, *ACS Sustainable Chem. Eng.* **2020**, *8*, 6466–6478; c) J. P. Hempfling, E. R. Sekera, A. Sarkar, A. B. Hummon, D. Pei, *J. Am. Chem. Soc.* **2022**, *144*, 21763–21771.

[18] a) L. Qiao, Z. Luo, R. Wang, X. Pei, S. Wu, H. Chen, T. Xie, R. A. Sheldon, A. Wang, *Green Chem.* **2023**, *25*, 7547–7555; b) R. Wang, J. Zhang, Z. Luo, T. Xie, Q. Xiao, X. Pei, A. Wang, *Int. J. Biol. Macromol.* **2022**, *205*, 682–691.

[19] a) R. X. Bai, B. L. Chen, L. Y. Zheng, *Microb. Cell Fact.* **2023**, *22*, 213; b) C. Dai, H. X. Cao, J. X. Tian, Y. C. Gao, H. T. Liu, S. Y. Xu, Y. J. Wang, Y. G. Zheng, *Biotechnol. Bioeng.* **2023**, *120*, 3543–3556; c) L. Qiao, Z. Y. Luo, H. M. Chen, P. F. Zhang, A. M. Wang, R. A. Sheldon, *Chem. Commun.* **2023**, *59*, 7518–7533.

[20] a) R. X. Fan, A. S. Aranko, *ChemBioChem* **2023**, e202300600; b) A. H. Keeble, M. Howarth, *Chem. Sci.* **2020**, *11*, 7281–7291; c) B. Zakeri, J. O. Fierer, E. Celik, E. C. Chittock, U. Schwarz-Linek, V. T. Moy, M. Howarth, *Proc. Natl. Acad. Sci. USA* **2012**, *109*, E690–E697.

[21] a) N. H. Schlieben, K. Niefind, J. Müller, B. Riebel, W. Hummel, D. Schomburg, *J. Mol. Biol.* **2005**, *349*, 801–813; b) K. Niefind, J. Müller, B. Riebel, W. Hummel, D. Schomburg, *J. Mol. Biol.* **2003**, *327*, 317–328.

[22] M. J. Lajoie, A. J. Rovner, D. B. Goodman, H.-R. Aerni, A. D. Haimovich, G. Kuznetsov, J. A. Mercer, H. H. Wang, P. A. Carr, J. A. Mosberg, N. Rohland, P. G. Schultz, J. M. Jacobson, J. Rinehart, G. M. Church, F. J. Isaacs, *Science* **2013**, *342*, 357–360.

[23] J. Zhang, R. Wang, Z. Y. Luo, D. M. Jia, H. M. Chen, Q. J. Xiao, P. F. Zhang, X. L. Pei, A. M. Wang, *Mater. Chem. Front.* **2022**, *6*, 182–193.

[24] W. Q. Zhou, T. Y. Gu, Z. G. Su, G. H. Ma, *Eur. Polym. J.* **2007**, *43*, 4493–4502.

[25] N. Kang, S. Yang, X. Xiong, A. Han, R. Ren, J. Wang, *Polymer* **2023**, *15*, 3478.

[26] B. A. Griffin, S. R. Adams, R. Y. Tsien, *Science* **1998**, *281*, 269–272.

[27] T. Bartoschik, S. Galinec, C. Kleusch, K. Walkiewicz, D. Breitsprecher, S. Weigert, Y. A. Muller, C. You, J. Piehler, T. Vercruysse, D. Daelemans, N. Tschammer, *Sci. Rep.* **2018**, *8*, 4977.

[28] a) T. Skóra, M. N. Popescu, S. Kondrat, *Phys. Chem. Chem. Phys.* **2021**, *23*, 9065–9069; b) S. Shin, H. S. Kim, M. I. Kim, J. Lee, H. G. Park, J. Kim, *Int. J. Biol. Macromol.* **2020**, *144*, 118–126; c) S. Kim, K. I. Joo, B. H. Jo, H. J. Cha, *ACS Appl. Mater. Interfaces* **2020**, *12*, 27055–27063; d) Q. Yang, B. Wang, Z. Zhang, D. Lou, J. Tan, L. Zhu, *RSC Adv.* **2017**, *7*, 38028–38036.

[29] a) J. C. Breger, J. N. Vranish, E. Oh, M. H. Stewart, K. Susumu, G. Lasarte-Aragonés, G. A. Ellis, S. A. Walper, S. A. Díaz, S. L. Hooe, W. P. Klein, M. Thakur, M. G. Ancona, I. L. Medintz, *Nat. Commun.* **2023**, *14*; b) I. Wheeldon, S. D. Minteer, S. Banta, S. C. Barton, P. Atanassov, M. Sigman, *Nat. Chem.* **2016**, *8*, 299–309; c) T. Man, C. Xu, X.-Y. Liu, D. Li, C.-K. Tsung, H. Pei, Y. Wan, L. Li, *Nat. Commun.* **2022**, *13*, 305.

Manuscript received: February 20, 2024
Accepted manuscript online: March 31, 2024
Version of record online: ■■, ■■

# Research Articles

## Multienzyme Cascades

Z. Luo, L. Qiao, H. Chen, Z. Mao, S. Wu, B. Ma, T. Xie, A. Wang, X. Pei,* R. A. Sheldon e202403539

Precision Engineering of the Co-immobilization of Enzymes for Cascade Biocatalysis

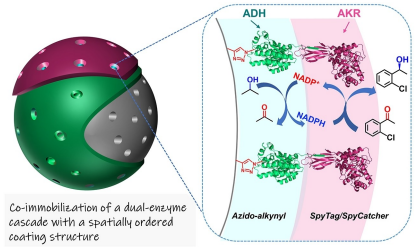


Co-immobilization of a dual-enzyme cascade with a spatially ordered coating structure

A double-layered coating approach was developed for the precise and sequential immobilization of dual-enzyme systems on resin particles using two biorthogonal counterparts of SpyTag/SpyCatcher and azide–alkyne cycloaddition. The method enables the combined purification and the ordered immobilization of enzymes and significantly enhances the catalytic efficiency and recyclability of multienzyme systems.